The Astrophysical Journal, 829:123 (14pp), 2016 October 1 doi:10.3847/0004-637X/829/2/123

NEW HALO STARS OF THE GALACTIC GLOBULAR CLUSTERS M3 AND M13 IN THE LAMOST DR1 CATALOG

Colin A. Navin[1,3], Sarah L. Martell[2], and Daniel B. Zucker[1,3,4]
[1] Department of Physics and Astronomy, Macquarie University, Sydney 2109, Australia; colin.navin@mq.edu.au, daniel.zucker@mq.edu.au
[2] School of Physics, University of South Wales, Sydney 2052, Australia; s.martell@unsw.edu.au
Received 2016 March 17; revised 2016 June 19; accepted 2016 June 20; published 2016 September 29

ABSTRACT

M3 and M13 are Galactic globular clusters with previous reports of surrounding stellar halos. We present the results of a search for members and extratidal cluster halo stars within and outside of the tidal radius of these clusters in the LAMOST Data Release 1. We find seven candidate cluster members (inside the tidal radius) of both M3 and M13, respectively. In M3 we also identify eight candidate extratidal cluster halo stars at distances up to ∼9.8 times the tidal radius, and in M13 we identify 12 candidate extratidal cluster halo stars at distances up to ∼13.8 times the tidal radius. These results support previous indications that both M3 and M13 are surrounded by extended stellar halos, and we find that the GC destruction rates corresponding to the observed mass loss are generally significantly higher than theoretical studies predict.

Key words: globular clusters: general – globular clusters: individual (M3 NGC 5272, M13 NGC 6205) – stars: kinematics and dynamics – techniques: radial velocities – techniques: spectroscopic

1. INTRODUCTION

Globular clusters (GCs) lose stars through both internal processes such as stellar evolution and two-body relaxation, and external influences such as tidal disruption, dynamical friction, and gravitational shocks due to passages close to the bulge and through the disks of their host galaxies. Consequently, at different epochs and even different points in their orbits, GCs may be less stable and have ex-member stars surrounding them or in associated tidal tail structures (e.g., Gnedin & Ostriker 1997; Vesperini 1997; Baumgardt & Makino 2003). The existence and properties of these extratidal stars can tell us how a GC has evolved since its formation via both internal dynamics and external influences of the host galaxy on the cluster (e.g., Chernoff et al. 1986; Gnedin & Ostriker 1997 and Vesperini 1997). It is necessary to understand these processes to understand the initial properties of the Galactic GC system. They can also tell us about the host galaxy itself in several ways. The lost stars contribute to a galaxy's stellar population, and observed tidal tails may be used as tracers of the galactic gravitational potential (e.g., Koposov et al. 2010 and Küpper et al. 2015). They can also be an indicator of the formation history of the host galaxy, as some GCs are believed to be part of dwarf galaxies that are accreted (e.g., Bellazzini et al. 2004; Mackey & Gilmore 2004; Carballo-Bello et al. 2011, 2014; Marino et al. 2014 and Da Costa 2015).

Grillmair et al. (1995) made the first discovery of Galactic GC tidal tails using automated star counts obtained from scanned UK Schmidt plates of 12 southern Galactic halo clusters. Likely cluster members on the main sequence, giant branch, and horizontal branch were selected within empirically determined color–magnitude envelopes. Obvious tidal structures were visible in the two-dimensional surface density maps they constructed. Subsequent studies have found evidence for tidal tails and/or surrounding stellar halos in over 30 other GCs (e.g., Leon et al. 2000; Grillmair & Dionatos 2006; Kunder et al. 2014; Navin et al. 2015, and Anguiano et al. 2016) and even in the GCs of the Andromeda Galaxy (M31) (Grillmair et al. 1996).

An indicator of the likelihood that GC stars will be found outside the tidal radius is the cluster destruction rate (or its inverse, the dissolution or destruction time). Significant simulations of the dynamical evolution of the Galactic GC system include Aguilar et al. (1988) and Hut & Djorgovski (1992). Gnedin & Ostriker (1997) calculated the total destruction rate of 119 GCs using simulations that included evaporation and disk and bulge gravitational shocks. They found that the present-day destruction time was similar to the typical GC age. To estimate how many GCs have been destroyed since the formation of the Galaxy, they favored a scale-free power law for the lifetime destruction rate. They concluded that the surviving population of GCs was a small fraction of those originally formed, and that a large fraction of the stars in the Galactic bulge and halo originated in GCs. A later study (Dinescu et al. 1999) of 38 GCs included proper motion data instead of statistically assigning velocities. They concluded that the orbits used in Gnedin & Ostriker (1997) were more destructive than are actually observed, so destruction rates for many clusters may have been overestimated. Mackey & Gilmore (2004) estimated that ∼100 of the present Milky Way (MW) GC population were formed in the Galaxy. Given that those with reasonably concentrated core radii ($r_c < 2$ pc) are less likely to be disrupted, they calculated that at least 50% of clusters have been destroyed over the last Hubble time. Mackey & van den Bergh (2005) estimated that the present population is 67% of the original, using observational differences in properties of "young halo," "old halo," and "bulge/disc" Galactic GC subsystems. Detailed simulations by Moreno et al. (2014) calculated orbits, tidal radii, and destruction rates due to bulge-bar and disk shocking for a sample of 63 Galactic GCs using six-dimensional data in axisymmetric and non-axisymmetric Galactic potentials, including a Galactic bar and a 3D model for the spiral arms.

[3] Astronomy, Astrophysics and Astrophotonics Research Centre, Macquarie University, Sydney, NSW, 2109, Australia.
[4] Australian Astronomical Observatory, P.O. Box 915, North Ryde, NSW 1670, Australia.

It is likely that a significant fraction of stars in the bulge and halo of the MW originated in GCs. Martell & Grebel (2010) studied the SDSS-II/SEGUE spectra of ~1900 G- and K-type halo giants and found that 2.5% showed abundance patterns only previously found in GC stars. They inferred that up to 50% of halo field stars initially formed within GCs. A further study (Martell et al. 2011) of 561 low-metallicity halo giant stars in SDSS-II/SEGUE 2 concluded, based on prevailing models of GC formation at the time, that a minimum of 17% of the present-day mass of the stellar halo originally formed in GCs.

GC tidal debris also acts as indicators of a host galaxy's gravitational potential as the extratidal stars spread out in a stream that traces the orbit of its progenitor. Recent work on this includes Küpper et al. (2015), who used the stellar stream associated with Pal 5 to constrain the Galactic mass within its apogalactic radius. Koposov et al. (2010) used the long narrow GD-1 stream of stars, likely to be from a defunct tidally disrupted GC, to constrain the circular velocity at the Sun's radius and the Galactic total potential flattening.

2. DATA AND INITIAL SELECTION PROCESS

There has already been a study searching for open and GC members (Zhang et al. 2015) in the LAMOST spectroscopic survey (Zhao et al. 2006). The survey footprint covers a number of Northern Hemisphere GCs, and therefore had potential as a data set to search for GC extratidal stars that have been observed in the program.

The LAMOST survey is a low/medium resolution spectroscopic survey of the Northern Hemisphere which aims to obtain the spectra of 10,000,000 objects, including stars, galaxies, and quasars. It uses the Guoshoujing Schmidt telescope located at the Xinglong Observatory in China. This telescope has a clear aperture of 4.0 m and a 5° field of view, with 4000 optical fibers of 3 arcsec diameter leading to 16 spectrographs. The spectral range is 3650–9000 Å with a limiting magnitude $r = 20$ at a resolution of $R = 500$.

Data Release 1 (DR1; Luo et al. 2015) contains data from the Pilot and First Year Surveys and is now publicly available for the general astronomical community. It contains 1,944,329 stellar spectra, with the DR1 AFGK Stars Catalog containing 1,061,918 high-quality spectra (later references in this paper to DR1 or the DR1 Catalog refer specifically to the DR1 AFGK Stars Catalog). As well as basic data such as positions and magnitudes from the input catalogs, these stars have values for stellar atmospheric parameters (effective temperature ($T_{\rm eff}$), surface gravity ($\log g$), and [Fe/H]) and heliocentric radial velocity ($V_{\rm r}$) derived using the LAMOST Stellar Parameter Pipeline (LASP).

Differentiating stellar cluster members from field stars is possible because cluster members are expected to share characteristics derived from their common origin. It is possible to identify candidate cluster members as a clump of stars in the parameter space defined by position, $V_{\rm r}$, stellar atmospheric parameters ($T_{\rm eff}$, $\log g$ and [Fe/H]), photometry, and proper motions. The gold standard for identification is detailed abundance matching from high-resolution spectroscopy, but large samples of candidates need to be cleaned in order to produce likely targets for this method.

Our first step was to identify target GCs that might have easily identifiable members or extratidal stars in the DR1 Catalog. We selected GCs within the survey area of LAMOST (decl. −10° to +90°) that had relatively high heliocentric radial velocities ($|V_{\rm r}| > 100\ {\rm km\ s^{-1}}$) to simplify differentiation of candidate stars from field stars in the same area of sky. There are 19 Northern Hemisphere GCs that satisfy these criteria. For each of these GCs we selected stars from the DR1 Catalog that were within a radius of 5° of the GC central position to encompass both a wide area within and outside the tidal radius, and that had a $V_{\rm r}$ within $\pm 20\ {\rm km\ s^{-1}}$ of the GC $V_{\rm r}$.

We found candidate stars in the DR1 Catalog around 10 GCs that satisfied these criteria: NGC 4147, M3, NGC 5466, M13, NGC 6229, M92 (NGC 6341), NGC 6426, NGC 6535, NGC 7078, and Pal 2. We discarded seven clusters as potential targets as they either had very few candidate stars or their $V_{\rm r}$ did not sufficiently differentiate them from the bulk of surrounding field stars. The three remaining GCs (M33, M13, and NGC 6229) had both a significant number of potential candidate stars and a $V_{\rm r}$ that was significantly distinct from field stars in the sky area.

Finally, we also rejected NGC 6229 as a potential target as the DR1 Catalog stars within a 5° radius of the GC central position are brighter than the cluster RGB. LAMOST exposes bright, medium, and faint plates that result in cuts at $r = 14$, 16, and 19 mag, respectively. All the DR1 Catalog stars in this sky area that satisfied the $V_{\rm r}$ criteria are brighter than $V = 16$, but on the V versus $V - K$ CMD the cluster RGB (defined by a PARSEC isochrone; Bressan et al. 2012) is mostly fainter than $V = 16$. It is likely that no faint fields were taken in this sky area during observations for DR1, and hence there are no likely members of NGC 6229 in the DR1 Catalog. Although we found a number of potential candidate stars based on $V_{\rm r}$, because we were not solely relying on radial velocity for selection we excluded those stars that were not consistent with the cluster RGB.

We investigate the two remaining clusters, M3 and M13, in this study. From initial samples of candidate stars for M3 and M13 selected by $V_{\rm r}$ and position (Section 4), we utilize photometry, $\log g$ and $\log(T_{\rm eff})$ (Section 5), proper motions (Section 6), and metallicities (Section 7) to clean our samples. We look at the spatial distribution of the candidate member samples with respect to the adopted tidal radii in Section 8 and present and discuss the final list of candidate cluster members and cluster halo stars in Section 9.

3. M3 AND M13 BACKGROUND

Both M3 and M13 are extremely well-studied observationally (e.g., both are in the SDSS footprint) and theoretically, and both have a complicated history regarding the possibility of extratidal stars. Searches (see below) for the existence of surrounding stellar halos outside the tidal radius for M3 have only sometimes been successful; observationally the case for extratidal stars around M13 is stronger. The search of Zhang et al. (2015) for both open and GC members in the LAMOST Data Release 2 (DR2) found M3 and M13 as the only two GCs with identified cluster members. Basic data for both clusters are presented in Table 1.

M3 was one of the GCs studied in a search for tidal tails by Leon et al. (2000). Member stars on Schmidt plates were identified using CMDs, and a star-count analysis was performed on the selected cluster stars. All 20 clusters analyzed showed evidence of tidal tails with projected directions preferentially toward the Galactic center. M3 showed evidence of an extension perpendicular to the Galactic plane, with the

Table 1
Basic Data on M3 and M13

	V_t (mag)	$R_\odot$ (kpc)	R_{gc} (kpc)	[Fe/H]	V_r (km s^{-1})	$\mu_\alpha\cos(\delta)$ (mas yr^{-1})	μ_δ (mas yr^{-1})	c (arcmin)	r_c (arcmin)	r_t (arcmin)
M3 (NGC 5272)	6.19	10.2	12.0	−1.53	−147.6	−1.1	−2.3	1.89	0.37	28.7
M13 (NGC 6205)	5.78	7.1	8.4	−1.50	−244.2	−0.9	5.5	1.53	0.62	21.0

Note. Data from Harris (1996) (2010 edition) catalog. V_t is the integrated V magnitude of the cluster. Proper motions $\mu_\alpha\cos(\delta)$ and μ_δ from Dinescu et al. (1999). Central concentration (c) and core radius (r_c) from McLaughlin & van der Marel (2005); tidal radius (r_t) calculated from $c = \log\frac{r_t}{r_c}$.

caveat that features in the cluster's density contours may have been introduced by contamination of the stellar sample. The most important mass-loss process, based on the shape of the tidal tail as well as the GC's position, orbit, and proper motion, was disk shocking. They noted that the importance of the interaction of GCs and the Galaxy was underlined by the detection of tidally stripped stars. However, later studies have found ambiguous evidence for the existence of extratidal stars around M3. Grillmair & Johnson (2006) used optimally filtered star counts for SDSS photometry, but found no evidence for tidal streams. Jordi & Grebel (2010) also used SDSS photometry with a color–magnitude weighted counting algorithm to search for extratidal features. They controlled carefully for sample contamination by background galaxies and quasars as well as dust extinction. The number density profile for M3 did not show any change in slope, hinting at an extratidal halo, and density contours did not reveal any large-scale tidal structure. They noted that this result was consistent with the Gnedin & Ostriker (1997) simulations. However, Chen & Chen (2010) used star-count analysis of the brighter members in the outer part of 116 Galactic GCs in the 2MASS (Skrutskie et al. 2006) Point Source Catalog. They listed M3 as 1 of 31 GCs that exhibited outlying filamentary or clumpy density enhancements, indicating the presence of stripped stellar members. This clumpiness was not, however, consistent with that found by Leon et al. (2000), and they did note that some clumpiness could arise from statistical fluctuations. Carballo-Bello et al. (2014) used both cross-correlation and isochrone fitting methods on wide-field photometric data from a variety of sources on a sample of 23 GCs. They were searching for evidence of an accretion origin for the GCs in the form of residual debris around the clusters from their now-defunct host dwarf galaxies. They reported no detections of any surrounding extratidal stellar structure around M3 and 13 other GCs, indicating that these GCs were not accreted along with a host dwarf galaxy. They noted that an early accretion time or low mass of an original host dwarf galaxy would also reduce the likelihood of the presence of extratidal stars and so did not rule out this scenario entirely.

M3 has a perigalacticon of 5.5 ± 0.8 kpc and is 12.0 kpc from the Galactic center, quite close to its apogalacticon of 13.7 ± 0.8 kpc (Dinescu et al. 1999). In theoretical studies, the previously cited Gnedin & Ostriker (1997) paper calculated total destruction rates for M3. For an isotropic GC system distribution with a Weinberg adiabatic conservation factor for the shock processes, they quote 3.98×10^{-12} and 5.42×10^{-12} yr^{-1} for two different Galactic models. This was ∼2 orders of magnitude less than the median destruction rates for their sample of 119 GCs for the same setup. Moreno et al. (2014) calculated the total destruction rate due to bulge-bar and disk shocking for M3. Depending on the models used this ranged from 1.62×10^{-12} to 2.97×10^{-12} yr^{-1}, somewhat lower than their median values. Both these studies indicate that M3 is relatively stable, with expected low rates of star loss.

The case for M13 is somewhat stronger observationally, with a number of searches finding evidence for extratidal stars. Lehmann & Scholz (1997) used automated star counts on scanned Schmidt plates to obtain projected density profiles and calculate structural parameters such as the tidal radii of seven GCs. They found that M13 (and other GCs) showed evidence of tidal tails in the form of increased surface density outside the calculated tidal radius of 23.8 arcmin. The previously cited Leon et al. (2000) study also included M13. They were not able to search over a very large sky area, but inside their adopted tidal radius of 56 pc they noted an extension toward the Galactic center in plots of density contours. Bulge shocking was considered to be the most likely process that would cause any loss of stars. Jordi & Grebel (2010) also detected a halo of extratidal stars extended slightly in the direction of motion in a similar position as the disturbed contours noted in Leon et al. (2000). The previously cited Chen & Chen (2010) study found M13 also showed possible outlying clumpy stellar debris. As with M3, this structure did not correspond with that found by the Leon et al. (2000) study.

M13 has an apogalacticon of 21.5 ± 4.7 kpc and is currently located reasonably close to its perigalacticon of 5.0 ± 0.5 kpc (Dinescu et al. 1999) at a distance of 8.4 kpc from the Galactic center. Gnedin & Ostriker (1997) quoted total destruction rates for M13 of 1.47×10^{-11} and 1.02×10^{-11} yr^{-1} for their two different galactic models. These are more than an order of magnitude less than the sample median destruction rate. The destruction rates calculated by Moreno et al. (2014) for M13 were, however, much lower at 6.20×10^{-14} to 1.04×10^{-13} yr^{-1}. As with M3, these theoretical studies show that M13 is expected to be relatively stable.

4. HELIOCENTRIC RADIAL VELOCITIES

The first panels of Figures 1 and 2 show V_r histograms of all the observed stars, with the predicted V_r distribution of the MW model (see below) generated by the Galaxia code (Sharma et al. 2011), overplotted as a gray histogram.

There were 4426 entries within a radius of 5° of the central position of M3 in the DR1 Catalog; 547 stars (∼14%) were duplicates (observed multiple times), leaving 3879 unique stars. For M13 there were 8265 entries within a radius of 5° of the central position; 910 stars (∼12%) were duplicates leaving 7355 unique stars. These numbers are consistent with the DR1 Catalog in general where ∼18% of the targets in total have been observed more than one time (Luo et al. 2015).

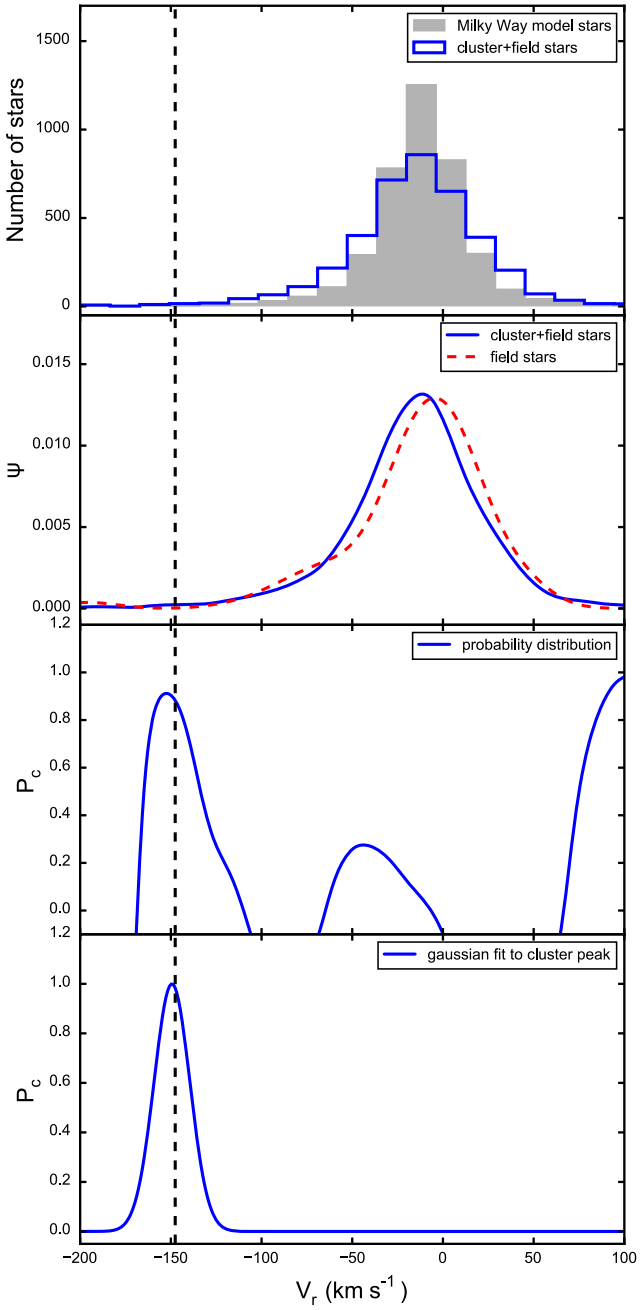

Figure 1. First panel: histogram of all the observed stars within a radius of 5° of M3's central position with the predicted V_r distribution of the Milky Way model generated by the Galaxia code (Sharma et al. 2011) overplotted as a gray histogram. Second panel: the solid blue line and the dashed red line show the Gaussian KDEs of the V_r of the observed stars and the field stars, respectively. Third panel: the solid blue line shows the V_r membership probability distribution. Fourth panel: the solid blue line shows the Gaussian fit to the cluster peak. The vertical dashed line shows the GC V_r.

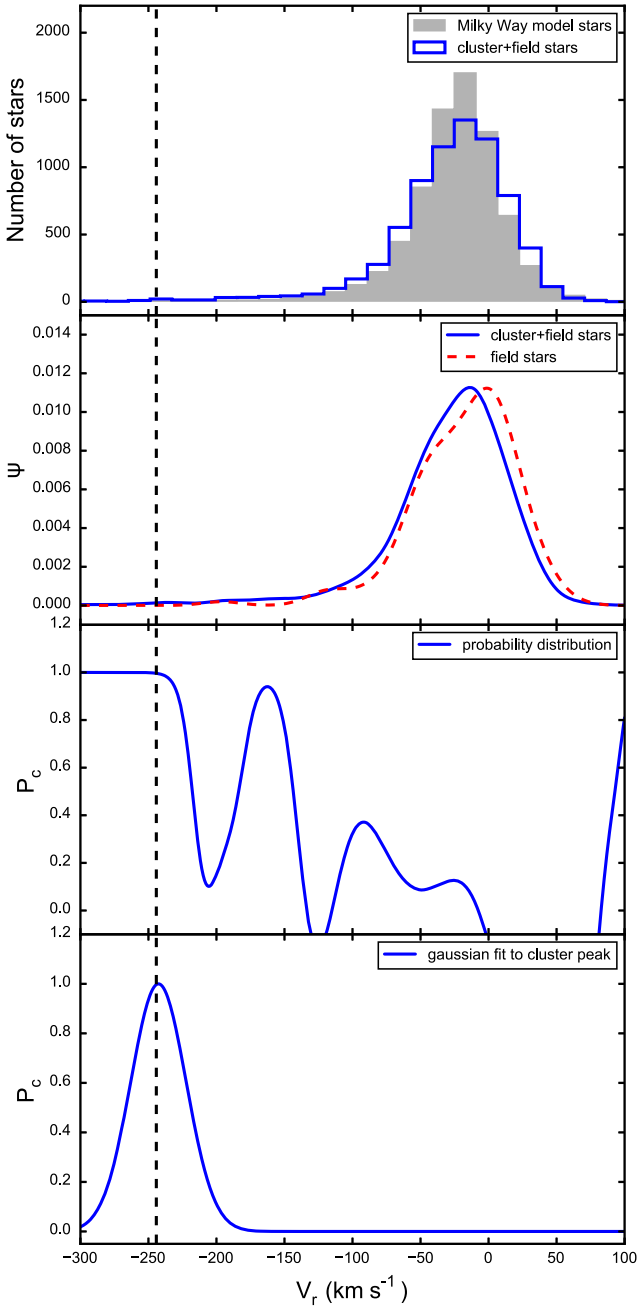

Figure 2. Same as Figure 1, but for M13.

For the duplicate stars we calculated V_r (and also $T_{\rm eff}$, $\log g$, and [Fe/H] below) from the DR1 values by taking a mean weighted by the respective errors, e.g.,

$$\overline{V_r} = \frac{\sum V_i/\delta_i^2}{\sum 1/\delta_i^2} \quad (1)$$

where V_i is the ith V_r and δ_i is the corresponding ith error.

We calculated a simple quadrature error in the parameter by, e.g.,

$$\overline{\Delta V_r} = \frac{\sqrt{\sum \delta_i^2}}{\sqrt{N}}, \quad (2)$$

where N is the number of observations of the star.

We used the Galaxia code to generate a synthetic catalog of stars to compare with the observations. Galaxia predicts radial velocities, metallicities, and other properties of a stellar sample given color, magnitude, and spatial constraints. We used the Besançon MW model (Robin et al. 2003) for the disk and the simulated N-body models of Bullock & Johnston (2005) for the stellar halo. We generated 10 models covering a 5° radius around the cluster center position with no color or magnitude

restrictions. The LAMOST observational target catalog selection strategy (Luo et al. 2015) is complex and, of course, for many practical reasons an input catalog may differ from the eventual products of a survey. Therefore, pragmatically, we used a simple magnitude cut ($9.0 \leqslant J \leqslant 12.5$) to construct the final V_r distribution. Finally, we summed and normalized the V_r distributions to have the same number of stars as the number of observed stars.

The sample of 3879 unique stars for M3 has a mean and standard deviation of the V_r distribution of $\overline{V_r} \sim -16 \pm 0.6$ km s^{-1} and $\sigma_{V_r} \sim 40 \pm 0.5$ km s^{-1}, respectively. In comparison the average MW model distribution has $\overline{V_r} \sim -13 \pm 0.5$ km s^{-1} and $\sigma_{V_r} \sim 30 \pm 0.3$ km s^{-1}. For the 7355 unique stars in the M13 sample, $\overline{V_r} \sim -29 \pm 0.6$ km s^{-1} and $\sigma_{V_r} \sim 48 \pm 0.4$ km s^{-1}; the corresponding figures for the model are $\overline{V_r} \sim -25 \pm 0.4$ km s^{-1} and $\sigma_{V_r} \sim 38 \pm 0.3$ km s^{-1}. Both distributions show a prominent peak near the mean V_r that we identify as predominantly Galactic disc or halo field stars (non-cluster members) plus an (unknown) number of cluster members.

We applied offsets to the V_r values in the DR1 Catalog to correct for systematic errors between the DR1 Catalog and the MWSC catalog (Kharchenko et al. 2013) noted in Zhang et al. (2015). For M3, the offsets are in the sense DR1 V_r—Harris (1996) $V_r = -6.4$ km s^{-1}, and for M13 the offsets are in the sense DR1 V_r—Harris (1996) $V_r = -6.9$ km s^{-1}.

We calculated the cluster membership probabilities P_c of stars on the basis of V_r using the method of Frinchaboy & Majewski (2008). We assumed that stars between two and three times the r_t of the cluster central position produced a sample of non-member field stars in the sky area of the cluster. There are 136 and 147 stars in these field samples for M3 and M13, respectively. However, as we were looking for extratidal stars that might well be in this sky area, it is possible to improve the field sample by removing stars that we already suspect are associated with the cluster. For M3 there is one star between two and three times the r_t with V_r within ± 20 km s^{-1} of the GC V_r, so we removed that star from the field sample. This left 135 stars in the field samples for M3.

First we made smoothed kernel density estimates (KDEs), i.e., the histograms were convolved with Gaussians with widths set by the measurement errors of (i) ψ_{c+f}—the complete V_r distribution (i.e., cluster stars plus field stars out to a radius of 5° from the cluster center), and (ii) ψ_f—the V_r distribution of field stars between two and three times the r_t. This is shown in the second panels on Figures 1 and 2. The formula for membership probability used by Frinchaboy & Majewski (2008) is

$$P_c = \frac{\psi_{c+f} - \psi_f}{\psi_{c+f}}. \quad (3)$$

The membership probability distributions are shown in the third panels of Figures 1 and 2.

We then applied Gaussian fits to the distributions around the cluster peaks in V_r (fourth panel of Figures 1 and 2). The KDE of field stars was extremely small in the region of both cluster peaks so the membership probability was very sensitive to that value. This resulted in probability values slightly in excess of one near the peak of the distribution, so we normalized the distributions so that the maximum values at the peaks were one. We then used the standard deviations (σ) of these Gaussian fits to select candidate cluster members that were within $\pm 2\sigma$ of the GC V_r and to determine their membership probabilities.

The mean and standard deviations of the Gaussian fit to the cluster peak for M3 for V_r are -152.7 and 15.4 km s^{-1}, respectively; the literature V_r is -147.6 ± 0.2 km s^{-1}. For M13 the mean and standard deviation are -242.8 and 20.0 km s^{-1}, respectively; the literature V_r is -244.2 ± 0.2 km s^{-1}. Members and extratidal halo stars of a GC are expected to share its V_r signature, so for initial samples of candidate cluster members on the basis of V_r we selected stars that were within $\pm 2\sigma$ of the GC V_r.

For M3 there are 57 stars in the DR1 Catalog that are within $\pm 2\sigma$ of the GC V_r and inside a radius of 5° of the GC central position. Seven of these stars are duplicates (each observed twice) and so we calculated mean parameter values and errors for these stars as above. This left a sample of 50 unique stars that we refer to as our M3 candidate stars. The mean and standard deviation of the V_r distribution of the candidate stars are -137.6 and 15.4 km s^{-1}. The V_r of these stars suggests that they are possibly cluster members or cluster halo stars. Our MW model predicts ~18 stars in the same area of sky within $\pm 2\sigma$ of the GC V_r that have no relation to the cluster and would therefore result in false positives, so we also used other parameters to further clean the sample.

There are 67 stars with 6 duplicates within $\pm 2\sigma$ of the V_r and within 5° of the GC central position for M13. The mean and standard deviation of the V_r distribution of the 61 unique stars left as our M13 candidate stars are -236.8 and 20.0 km s^{-1}, respectively. As with M3, their V_r suggests that these stars are possibly cluster members or cluster halo stars; for M13 our MW model predicts a sample contamination of ~28 stars.

Many DR1 catalog V_r errors are fairly large for the stars selected by V_r for both clusters. Typical errors in V_r are quoted as 5 km s^{-1} (Zhang et al. 2015); however, the mean V_r error for our candidate members for M3 is 15.2 km s^{-1} and for M13 it is 17.1 km s^{-1}, similar to the standard deviation of the V_r distribution of the candidate stars. Therefore, it is likely that the errors of the LAMOST radial velocities are the largest contributor to the dispersion in the Gaussian fits to the cluster peaks.

5. PHOTOMETRY AND STELLAR PARAMETERS (SURFACE GRAVITY AND EFFECTIVE TEMPERATURE)

Photometric data were obtained from the UCAC4 catalog (Zacharias et al. 2013) containing V magnitudes from APASS (Henden et al. 2009) and K_s magnitudes from 2MASS (Skrutskie et al. 2006). Figure 3 shows the V versus $V - K_s$ CMD and the $\log(T_{\rm eff})$ versus $\log g$ diagrams for the 50 unique M3 candidate stars. The plots also show the PARSEC isochrone (Bressan et al. 2012) generated for M3. Input parameters for producing the isochrone are age 12.6 Gyr from the Milky Way Star Clusters (MWSC) catalog (Kharchenko et al. 2013); [Fe/H] $= -1.50$; $[\alpha/\mathrm{Fe}] = 0.3$ (Marin-Franch et al. 2009) $\Rightarrow Z = 0.0079$; $E(B - V) = 0.01 \Rightarrow A_v = 0.032$; apparent visual distance modulus $(m_v - M_v) = 15.07$. The V magnitude of the horizontal branch $V_{\rm HB}$ is 15.64 and this agrees with its position on the V versus $V - K$ CMD.

The V versus $V - K_s$ CMD and the $\log(T_{\rm eff})$ versus $\log g$ diagrams for the 61 unique M13 candidate stars are shown in Figure 4. Input parameters for generating the PARSEC isochrone are age 12.6 Gyr from the MWSC catalog (Kharchenko et al. 2013); [Fe/H] $= -1.53$; $[\alpha/\mathrm{Fe}] = 0.3$ (Marin-

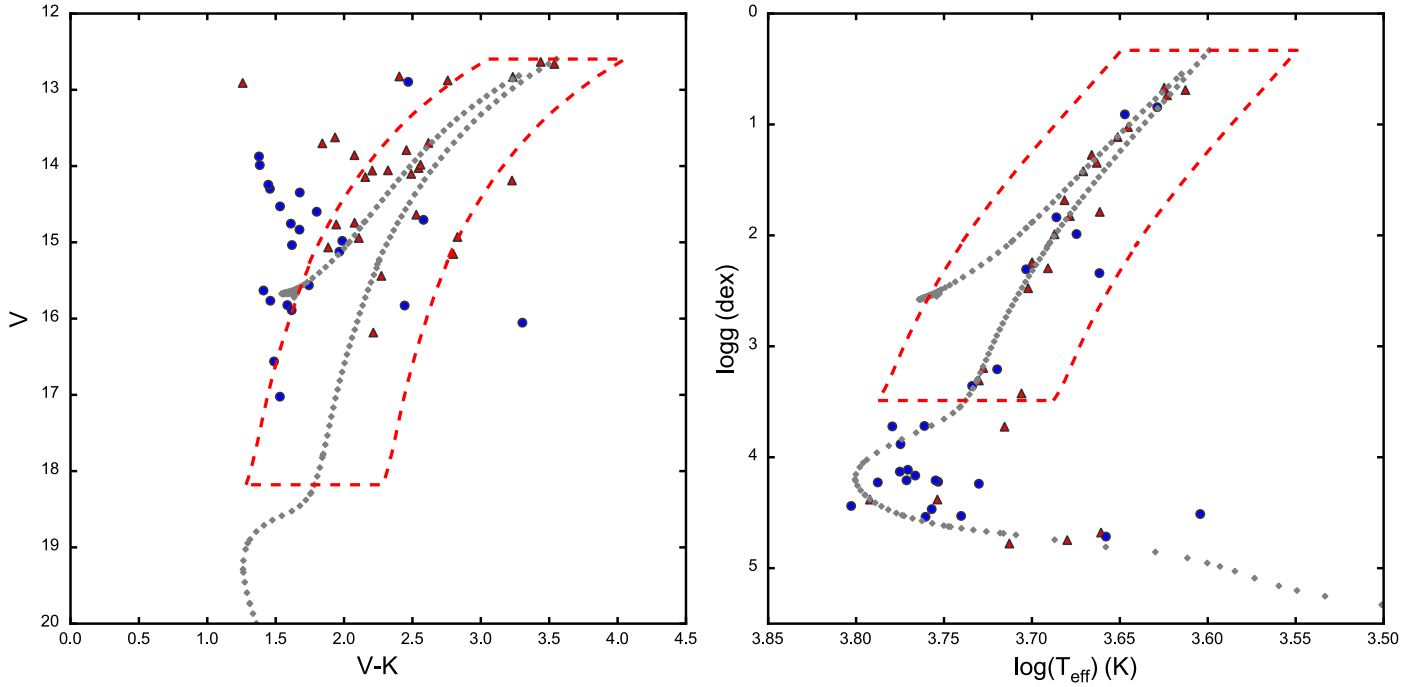

Figure 3. Left-hand panel: V vs. $V - K_s$ CMD of candidate stars around M3. Right-hand panel: log($T_{\rm eff}$) vs. log g diagram of candidate stars. The gray diamonds show the PARSEC isochrone (Bressan et al. 2012) for the GC. In the left panel the dashed red line shows the boundary for candidate selection based on V vs. $V - K_s$ photometry. The stars are color-coded with red triangles as the stars that are inside the $T_{\rm eff}$ vs. log g limits box (the red dashed box on the right panel) and blue circles as stars outside the $T_{\rm eff}$ vs. log g limits box. In the right panel the dashed red line shows the boundary for candidate selection based on $T_{\rm eff}$ vs. log g. The stars are color-coded with red triangles as stars that are inside the V vs. $V - K_s$ limits box (the red dashed box on the left panel) and blue circles as stars that are outside the V vs. $V - K_s$ limits box.

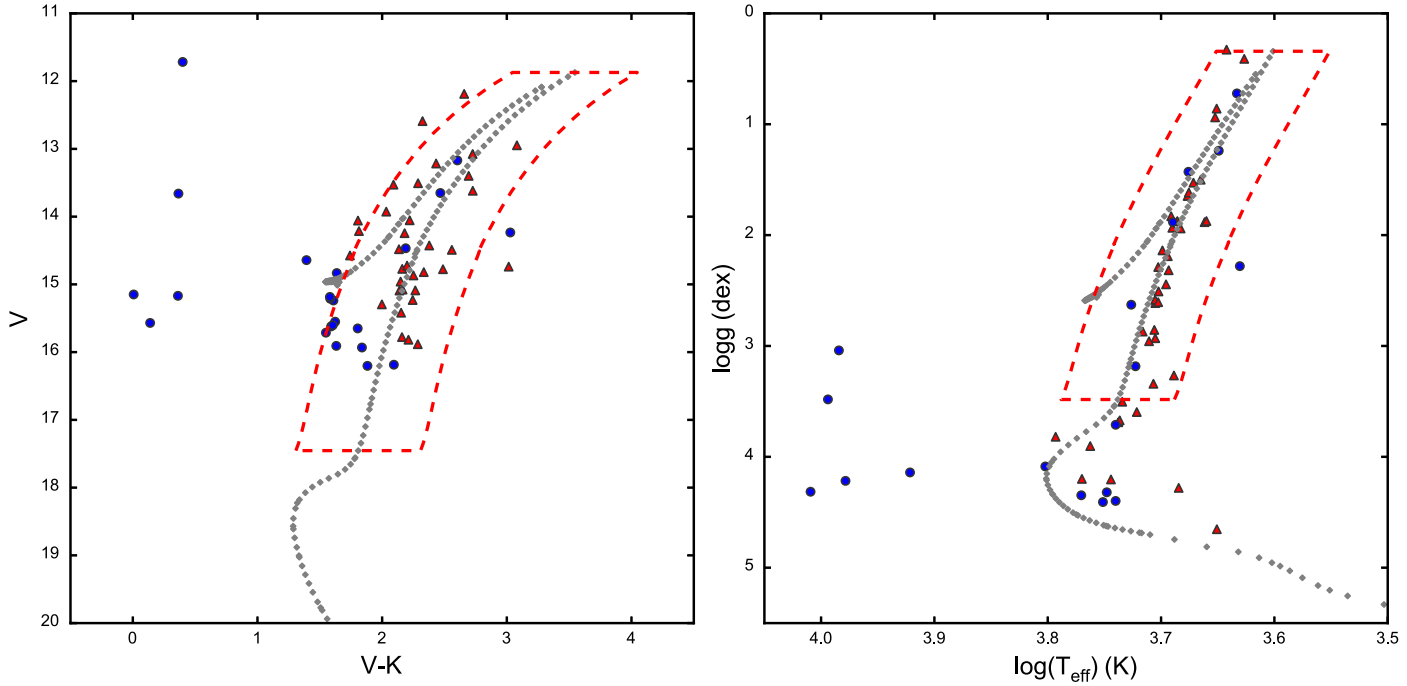

Figure 4. Same as Figure 3 for M13.

Franch et al. 2009) $\Rightarrow$ $Z = 0.0073$; $E(B - V) = 0.02 \Rightarrow A_v = 0.064$; apparent visual distance modulus $(m_v - M_v) = 14.33$. V_{HB} is 14.90 and this agrees with its position on the V versus $V - K$ CMD.

For both clusters, the magnitudes of observed stars and the positions of the isochrones on the CMDs show that any GC members must be giants and that any dwarfs observed are foreground stars rather than cluster members. Therefore, our V versus $V - K$ and log($T_{\rm eff}$) versus log g limits were based on selecting stars close to the RGB.

The dashed red lines on the left panel show the V versus $V - K_s$ boundaries we adopted for candidate selection with

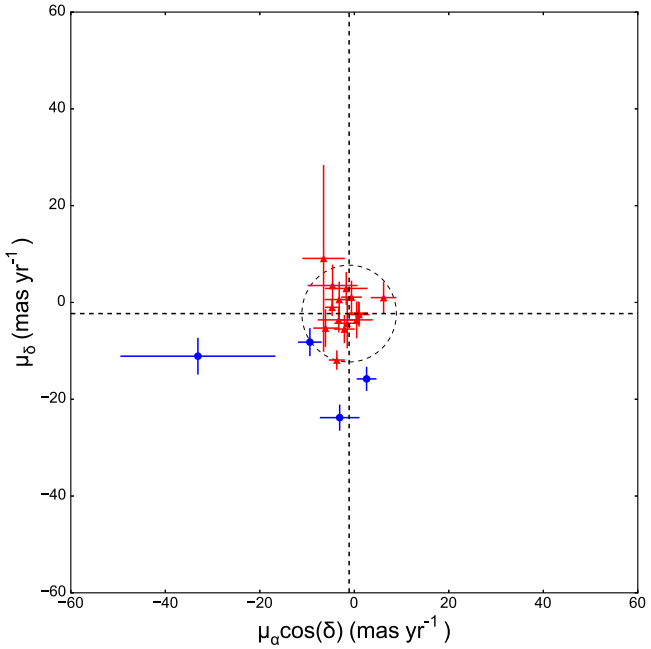

Figure 5. Absolute proper motions of the candidate stars of M3. Red triangles denote stars outside the tidal radius with proper motions within 10 mas yr^{-1} of the GC proper motion, or stars that are inside the tidal radius. Blue circles denote stars outside the tidal radius that have proper motions more than 10 mas yr^{-1} different from the GC proper motion. The vertical and horizontal black dashed lines indicate the GC proper motion and the black dashed circle indicates the 10 mas yr^{-1} limit.

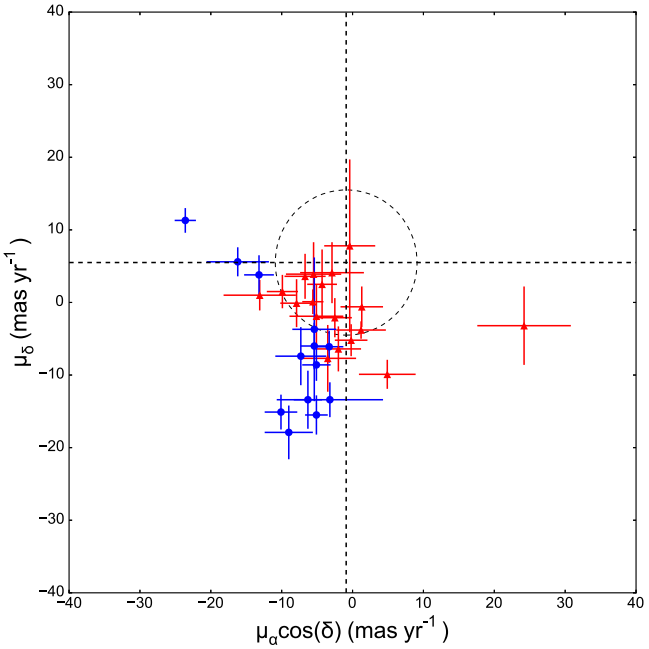

Figure 6. Same as Figure 5, but for M13.

respect to the isochrone for M3. The boundaries are ± 0.5 mag in $V - K_s$ and $12.6 < V < 18.2$ mag to incorporate the V magnitude range of the RGB. The dashed red lines on the right panel show the $\log(T_{\rm eff})$ versus $\log g$ boundaries we adopted. This incorporates a cut at $\log g = 3.5$ to separate dwarfs from giants and the width of the box is ± 0.05 in $\log(T_{\rm eff})$. Altogether we removed 31 stars that were outside either of these boundaries.

For M13 we adopted boundaries for the photometric selection of ± 0.5 mag in $V - K_s$ and $11.9 < V < 17.5$ mag and for the $\log(T_{\rm eff})$ versus $\log g$ boundaries we adopted the same cut at $\log g = 3.5$ and again the width of the box is ± 0.05 in $\log(T_{\rm eff})$. We removed 29 stars from the list of candidates based on these boundaries.

6. PROPER MOTIONS

Observed proper motions can also be used to clean a sample of candidate stars if their proper motions do not match that of the cluster. For our purposes we adopted a limit of 10 mas yr^{-1} of the GC proper motion. However, because it is difficult to make proper motion measurements in crowded stellar fields, we discounted proper motion as a necessary condition for membership for the candidate stars inside the tidal radius.

We obtained the absolute proper motions of all 19 remaining candidate stars of M3 from the UCAC4 catalog (Zacharias et al. 2013) and the GC proper motion ($\mu_\alpha \cos(\delta) = -1.1 \pm 0.51$ mas yr^{-1}, $\mu_\delta = -2.3 \pm 0.54$ mas yr^{-1}) from Dinescu et al. (1999). Figure 5 shows a plot of the absolute proper motions of the candidate stars. For stars outside the tidal radius, we accepted stars with proper motions that are within 10 mas yr^{-1} of the GC proper motion (black dashed circle on Figure 5). Four of the 19 candidate stars that are outside the GC tidal radius had proper motions more than 10 mas yr^{-1} different from the GC proper motion, so we eliminated these as candidates. We did not discount any stars that are inside the tidal radius as potential members on the basis of their proper motions. There were seven stars inside the tidal radius and we kept all these stars as candidates.

UCAC4 has absolute proper motions for 31 of the 32 candidate stars of M13. The GC proper motion of the GC is $\mu_\alpha \cos(\delta) = -0.9 \pm 0.71$ mas yr^{-1}, $\mu_\delta = 5.5 \pm 1.12$ mas yr^{-1} (Dinescu et al. 1999). Figure 6 shows a plot of the absolute proper motions of the candidate stars. We eliminated 13 of the 25 stars that are outside the GC tidal radius with proper motions more than 10 mas yr^{-1} different from M13's proper motion. There were seven stars inside the tidal radius and we kept all these stars as candidates. We also retained in our list of candidates one star without proper motion data (obsid 50501031).

7. METALLICITIES

We applied offsets to the [Fe/H] values in the DR1 Catalog to correct for systematic errors between the DR1 Catalog and the MWSC catalog (Kharchenko et al. 2013) noted in Zhang et al. (2015), and the offsets in cluster [Fe/H] between the Harris (1996) catalog and the MWSC catalog (Kharchenko et al. 2013). The offsets are in the sense M3: DR1 [Fe/H]—Harris (1996) [Fe/H] $= -0.15$ dex; M13: DR1 [Fe/H]—Harris (1996) [Fe/H] $= -0.03$ dex.

Members and extratidal halo stars of a GC are expected to have a similar [Fe/H] to that of the cluster (for a review see Gratton et al. 2012) and most GCs, including M3 (Cohen & Meléndez 2005) and M13 (Cohen & Meléndez 2005 and Johnson & Pilachowski 2012) do not have a significant [Fe/H] spread. The quoted typical uncertainty in [Fe/H] for LAMOST spectra is 0.1–0.2 dex (Zhang et al. 2015), so we initially considered this as a limit for a star to have an [Fe/H] consistent with that of the cluster. However, the DR1 Catalog [Fe/H]

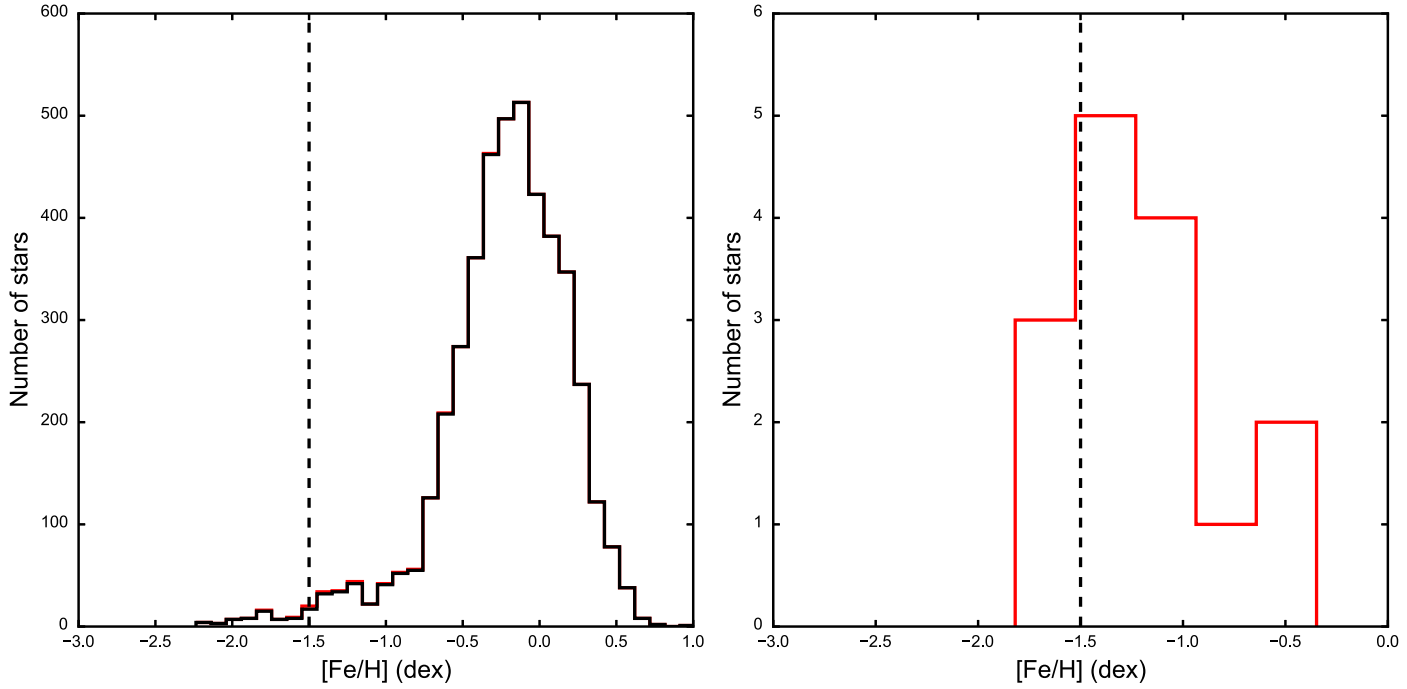

Figure 7. Left-hand panel: the black line shows the [Fe/H] distribution of observed stars within a 5° radius of the M3 central position. Right-hand panel: the red line shows the expanded [Fe/H] distribution of candidate stars. The vertical dashed line indicates the GC [Fe/H].

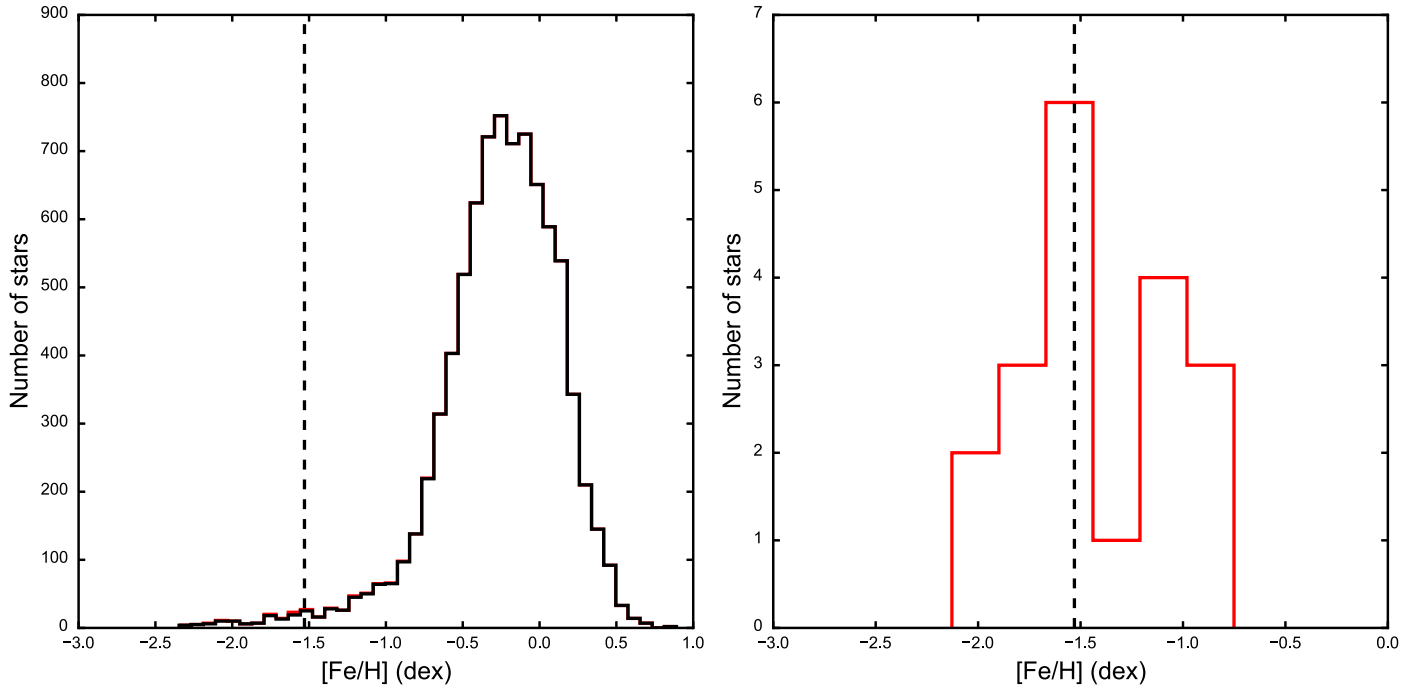

Figure 8. Same as Figure 7, but for M13.

errors for our candidates are generally considerably higher than this, ranging from 0.23 to 1.16 with a median value of 0.58 dex for M3 and 0.19 to 1.46 with a median value of 0.86 dex for M13.

No studies have shown any overall star-to-star [Fe/H] metallicity variations for M3 (Cohen & Meléndez 2005). Figure 7 shows the [Fe/H] distributions for M3. The left-hand panel shows all the observed stars within a radius of 5° of the GC central position. The distribution shows a prominent peak consisting of 3879 stars with a mean [Fe/H] ~ -0.22 dex that we predominantly identify as Galactic disk or halo field stars (non-cluster members). The right-hand panel of Figure 7 is an expanded version centered on the [Fe/H] of the GC showing only the 15 candidate stars. Values range from -1.82 to -0.35 dex. There are 12 of the 15 candidate stars within the median error (± 0.58 dex) of the GC [Fe/H] of -1.50 dex; the bulk of stars are more metal-rich than the cluster [Fe/H]. Values of [Fe/H] in Zhang et al. (2015) for member stars range from -2.09 to -1.1 dex; they did not eliminate any stars as possible members based on [Fe/H].

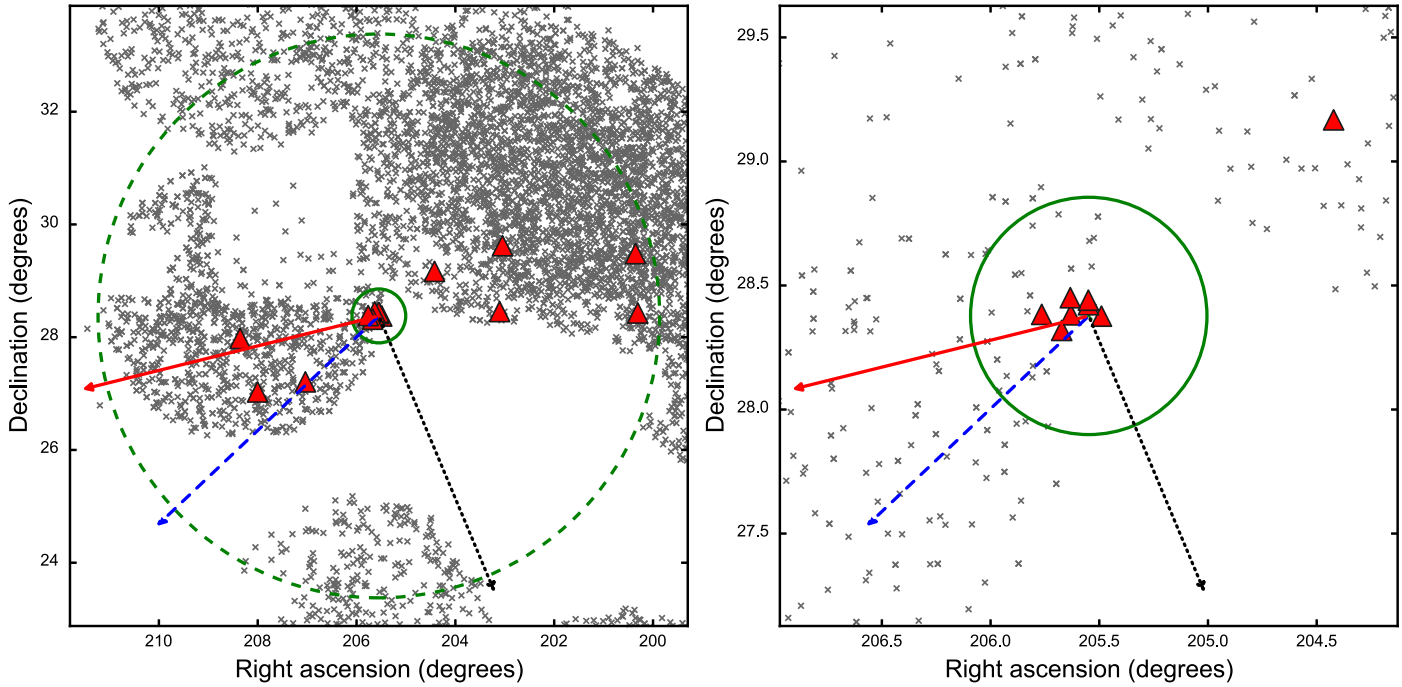

Figure 9. Left-hand panel: spatial distribution of DR1 Catalog stars around M3. Right-hand panel: expanded version showing the DR1 Catalog stars inside the tidal radius. Gray crosses show non-members, and red triangles denote candidate cluster member stars and candidate extratidal cluster halo stars. The green cross and solid circle show the center position and the tidal radius, respectively; the dashed circle is at a 5° radius from the center position. The black dotted arrow indicates the direction of the cluster proper motion, the blue dashed arrow is the direction to the Galactic center, and the solid red arrow is the direction perpendicular to the Galactic plane.

M13 is also not known to exhibit any overall [Fe/H] metallicity variations (Cohen & Meléndez 2005 and Johnson & Pilachowski 2012). The [Fe/H] distributions for M13 are shown in Figure 8. The main peak in the left-hand panel consists of 7355 stars with a mean [Fe/H] ~ -0.26 dex that we predominantly identify as non-cluster members. The right-hand panel of Figure 8 is an expanded version centered on the [Fe/H] of the GC showing only the 19 candidate stars. Values range from -2.13 to -0.75 dex. All 19 candidate stars are within the median error (± 0.86 dex) of the GC [Fe/H] of -1.53 dex. Zhang et al. (2015) again did not eliminate any stars on the basis of their [Fe/H]; values of member stars of M13 in their study range from -1.81 to -1.56 dex.

In view of the large ranges in [Fe/H] and the large errors in [Fe/H] of stars in our samples, we also chose not to eliminate any stars for either cluster based on [Fe/H]. The DR1 Catalog values of [Fe/H] as calculated by LASP do not seem to be helpful in this case. It would be desirable to revisit these limits in future with more precise abundance information.

8. SPATIAL DISTRIBUTION

Figure 9 shows the spatial (R.A.—decl.) distribution of observed and candidate stars for M3. Of the 15 final candidate stars, 8 are outside the adopted tidal radius of 28.7 arcmin at distances from the GC center ranging from ~2.6 to ~9.8 times the tidal radius. Seven candidate stars are inside the tidal radius and we recovered seven of the nine unique stars identified as cluster members in Zhang et al. (2015). There are a further two stars identified in that paper (based on DR2) that are not in the DR1 Catalog. The eight stars outside the adopted tidal radius are identified as candidate extratidal cluster halo stars. The stars appear to form a broadly symmetrical linear feature on both sides of the cluster, and it is possible that this is an indication of a tidal tail. However the alignment is roughly perpendicular to the direction of the cluster proper motion and the tails should be extended along the cluster orbit. It also appears to be somewhat aligned with the coverage of the fields, although the north–east quadrant looks fairly uniform. More complete sky coverage as the LAMOST survey continues should resolve this uncertainty.

The spatial distribution of stars for M13 is shown in Figure 10. There are 12 of the 19 candidate stars outside the adopted tidal radius of 21.0 arcmin. For these stars the distances range from ~4.3 to ~13.8 times the tidal radius. Seven of the candidate stars are inside the tidal radius and we recover all four of the stars identified as cluster members in Zhang et al. (2015). The 12 stars outside the adopted tidal radius are identified as candidate extratidal cluster halo stars.

9. FINAL MEMBER LIST AND DISCUSSION

There are a number of parameters that can be used to select candidate members of a GC from a field sample of stars. Here we had position, radial velocities, stellar atmospheric parameters ($T_{\rm eff}$, $\log g$ and [Fe/H]), photometry, and proper motions. We used $V_{\rm r}$ as the primary discriminant, but we have constructed a composite filter, based on all available information, that gives better member/non-member discrimination than any single parameter.

Our first step was to identify the characteristics of GCs that were likely to have member stars in the DR1 Catalog. Spatially they had to be within the survey area of LAMOST (decl. $-10°$ to $+90°$) and we then chose to use GCs that had relatively high heliocentric radial velocities ($|V_{\rm r}| > 100$ km s^{-1}). Stars from these GCs should have significantly different $V_{\rm r}$ to field stars in the same region of sky, and we made an initial search for stars with $V_{\rm r}$ within ± 20 km s^{-1} of the respective GC $V_{\rm r}$. To search

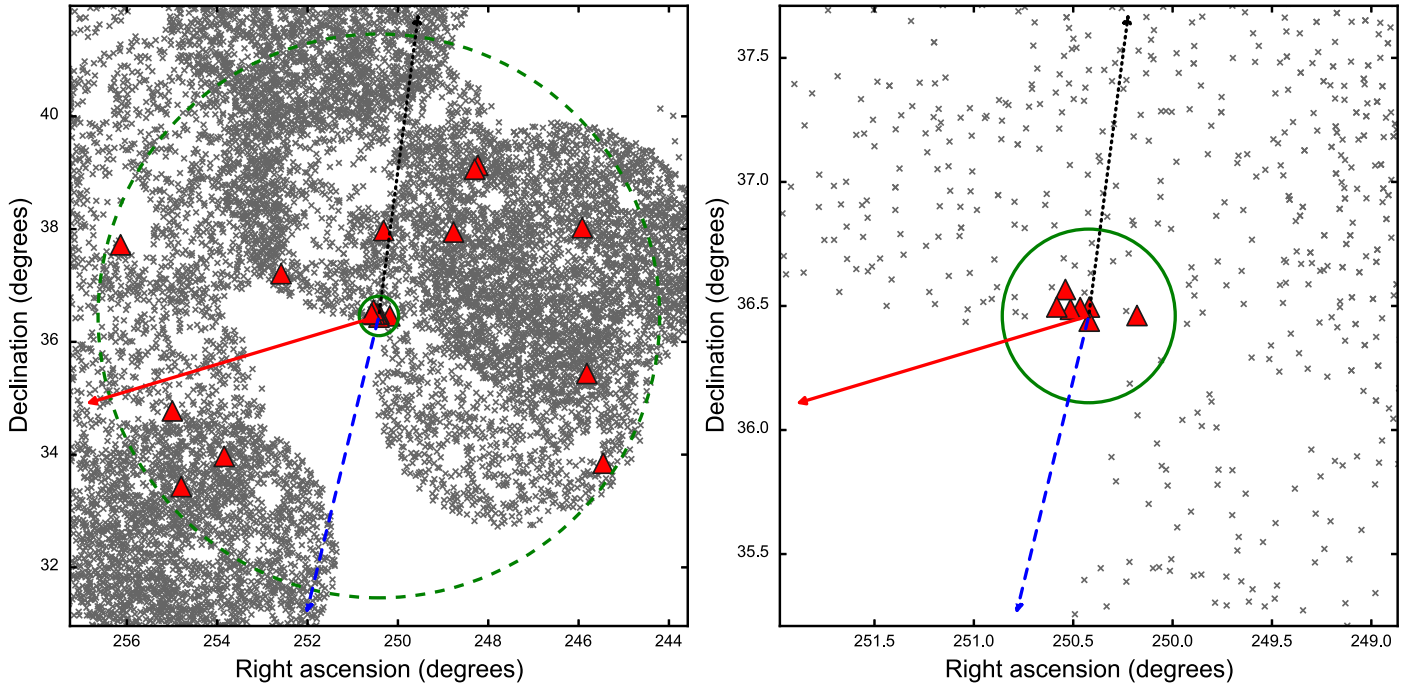

Figure 10. Same as Figure 9, but for M13.

for possible cluster halo stars or tidal tails well outside the GC tidal radius we chose a wide search area encompassing a radius of 5° from the GC central position. After eliminating GCs that only had small numbers of candidate stars, or where the differentiation between the GC V_r and field stars was not large or the observed stars were too bright to be cluster members, we were left with M3 and M13 as likely candidate GCs to search for extratidal stars.

The first criterion for selection as a cluster member was V_r. The range for selection was based on the standard deviation σ of Gaussian fits to probability distribution functions of V_r. M3 has 50 unique candidate members in LAMOST DR1 that are within a radius of 5° of the GC central position and that have a V_r within $\pm 2\sigma$ of the GC V_r. Based on V versus $V - K$ and log ($T_{\rm eff}$) versus log g limits, we eliminated 31 of these candidates. For the 19 remaining stars, there are 7 stars inside and 12 stars outside the tidal radius. For the 12 stars outside the tidal radius, 4 have high proper motions relative to the GC, and we accepted the remaining 8 stars with proper motions within 10 mas yr^{-1} of the GC proper motion. We discounted the DR1 Catalog [Fe/H] as a selection criterion. We identify the remaining eight stars as our final cluster halo member sample. Spatially these stars range from ∼2.6 to ∼10.2 times the tidal radius. For the seven stars inside the tidal radius we did not use proper motions so these stars are our final cluster members. We recovered all seven of the stars identified as cluster members in Zhang et al. (2015) that are in DR1. All the candidate member and extratidal halo stars are listed in Table 2; the final column gives their status as m = candidate cluster member star, h = candidate extratidal cluster halo star. Altogether we eliminated 35 stars out of the 50 that were selected on the basis of V_r alone, so this is not inconsistent with the predicted ∼18 stars unrelated to the cluster that would be in the same region of sky and within $\pm 2\sigma$ of the GC V_r from the MW model.

We identified 61 candidate members of M13 in LAMOST DR1 from radial velocities alone. We eliminated 29 of these candidates based on V versus $V - K$ and log($T_{\rm eff}$) versus log g limits and 13 based on proper motion limits. There are 12 of the remaining 19 stars are outside the tidal radius at distances ranging from ∼3.4 to ∼13.8 times the tidal radius and these stars make up our final candidate cluster extratidal halo sample. The seven stars inside the tidal radius make up our final cluster member sample. We recovered all four of the stars identified as cluster members in Zhang et al. (2015). We eliminated 42 stars out of the 61 stars that were selected on the basis of V_r alone and, again, this is reasonably consistent with our MW model predicted sample contamination of ∼28 stars. All the candidate member and extratidal halo stars are listed in Table 3, and the final column gives their status.

If these stars have indeed escaped from their parent clusters, it is of interest to compare the destruction rate that this implies to that of simulations such as Gnedin & Ostriker (1997) and Moreno et al. (2014).

To estimate the observed cluster fractional mass loss we used the ratio of the total cluster extratidal halo stars V luminosity to the integrated cluster V luminosity (from the cluster integrated V magnitude). The observed cluster fractional mass losses are 0.0038 and 0.0046 for M3 and M13, respectively. We then adjusted for sample completeness: (i) DR1 is not spatially complete (see Figures 9 and 10) over the area of sky we searched, and (ii) DR1 is not photometrically complete to the faintness limit of the RGB for these GCs. We estimated completeness as the ratio of the number of DR1 stars to samples of stars from the UCAC4 (Zacharias et al. 2013) catalog. For both LAMOST and UCAC4 we selected stars outside the GC tidal radius with a faint limit of $V < 16$ mag. The V magnitudes in UCAC4 are from APASS (Henden et al. 2009) so the limit was chosen to match the quoted current completeness of $V = 16$ mag. This gave a DR1 completeness of 0.209 and 0.143 for M3 and M13, respectively. The

Table 2
Candidate Cluster Members and Cluster Halo Stars of M3 (NGC 5272)

obsid	ID	R.A. (°)	decl. (°)	V (mag)	K_s (mag)	V_r (km s^{-1})	T_{eff} (K)	log g	[Fe/H]	$\mu_\alpha \cos(\delta)$ (mas yr^{-1})	μ_δ (mas yr^{-1})	R (arcmin)	P_c	Status
51313025	2MASS J13211409+2825469	200.308734	28.42971	16.18	13.97	−136.7	5012	2.2	−1.54	−3.2	0.6	276.5	0.79	h
145202042	2MASS J13212483+2928571	200.353534	29.48254	13.79	11.34	−117.7	4604	1.3	−1.00	−2.1	−5.5	280.7	0.02	h
145207028	2MASS J13321118+2937216	203.046613	29.62271	14.74	12.67	−121.0	5011	2.2	−0.60	−3.3	−3.6	151.1	0.06	h
48701211	2MASS J13322499+2827163	203.104159	28.45454	14.93	12.10	−131.6	4586	1.8	−0.81	1.0	−2.5	129.1	0.47	h
48707124	2MASS J13374132+2910037	204.422183	29.16770	14.77	12.82	−117.2	5081	3.4	−0.35	−1.5	−4.3	75.9	0.02	h
110310139	Cl* NGC 5272 SK 533	205.490031	28.37642	14.14	11.99	−153.2	4803	1.7	−1.49	−6.5	9.1	3.1	0.55	m
110310150	Cl* NGC 5272 SK 326	205.549885	28.42252	14.64	12.11	−148.5	4769	1.8	−1.38	−1.7	2.9	2.7	0.85	m
110210143	Cl* NGC 5272 SK 675	205.550218	28.44069	12.63	9.20	−147.6	4199	0.7	−1.17	−6.1	−5.3	3.8	0.89	m
110310142	Cl* NGC 5272 S 1104	205.630851	28.38177	13.70	11.08	−152.6	4419	1.0	−1.43	−4.6	3.5	4.4	0.59	m
110310134	Cl* NGC 5272 SK 68	205.633223	28.45072	13.98	11.42	−152.8	4480	1.1	−1.49	0.5	−3.6	6.3	0.58	m
110210146	Cl* NGC 5272 SK 26	205.672917	28.31891	12.66	9.12	−155.3	4099	0.7	−0.95	0.9	−2.2	7.4	0.42	m
110210131	2MASS J13430354+2823003	205.764840	28.38346	12.83	9.60	−148.6	4215	0.7	−1.22	−0.6	1.1	11.4	0.84	m
110202247	2MASS J13480854+2712278	207.035611	27.20771	14.10	11.61	−141.5	4635	1.3	−1.29	−3.7	−11.9	105.6	0.99	h
110201055[a]	2MASS J13520088+2701435	208.003680	27.02878	14.03	11.48	−153.0	4686	1.4	−1.82	−4.7	−1.0	153.5	0.56	h
110305113	2MASS J13532551+2758396	208.356275	27.97771	15.44	13.17	−149.2	4866	2.0	−1.57	6.2	1.0	150.4	0.80	h

Note. R = radial distance from cluster center.
P_c = membership probability based on V_r.
Status: m = candidate cluster member star; h = candidate extratidal cluster halo star.
Identifications are from Sandage (1953), Sandage & Katem (1982) or 2MASS.
[a] Duplicate of 110301055.

Table 3
Candidate Cluster Members and Cluster Halo Stars of M13 (NGC 6205)

obsid	ID	R.A. (°)	decl. (°)	V (mag)	K_s (mag)	V_r (km s^{-1})	T_{eff} (K)	log g	[Fe/H]	$\mu_\alpha \cos(\delta)$ (mas yr^{-1})	μ_δ (mas yr^{-1})	R (arcmin)	P_c	Status
154202032	2MASS J16214912+3350517	245.454661	33.84772	12.95	9.87	−262.2	4233	0.4	−2.13	1.2	−3.8	289.7	0.42	h
50501031	2MASS J16231617+3526204	245.817393	35.43900	–	13.51	−235.6	5200	2.4	−2.10	...	...	231.9	1.00	h
50515195	2MASS J16234061+3801295	245.919214	38.02485	15.88	13.60	−226.6	5081	2.9	−1.06	−6.7	3.6	234.6	0.90	h
50512192	2MASS J16325546+3907555	248.231107	39.13208	15.42	13.27	−267.9	4943	2.2	−1.49	−5.1	−1.9	191.0	0.28	h
46412198[a]	2MASS J16331239+3903510	248.301662	39.06417	15.09	12.82	−230.2	4737	1.6	−1.77	−5.5	3.9	185.8	0.96	h
50513129	2MASS J16350451+3756531	248.768818	37.94810	15.82	13.61	−216.8	4883	3.3	−0.93	−9.9	1.5	119.2	0.63	h
51801233	Cl* NGC 6205 SANDA A1	250.179108	36.46162	13.40	10.70	−241.5	4477	0.9	−1.58	−0.2	−5.2	11.7	0.96	m
51805041	2MASS J16411545+3758307	250.314372	37.97520	15.09	12.95	−221.2	4898	1.9	−1.56	−2.5	−2.1	91.1	0.76	h
51801212	2MASS J16414050+3629442	250.418656	36.49562	...	12.45	−245.7	5013	2.4	−1.54	24.2	−3.2	2.2	0.89	m
48801219	Cl* NGC 6205 BARN 123	250.419514	36.43891	...	12.06	−247.5	5404	2.6	−1.37	4.9	−9.9	1.3	0.84	m
48801215	Cl* NGC 6205 ARP 1054	250.464965	36.49338	...	11.55	−221.0	5115	2.0	−1.18	−13.1	1.0	2.9	0.76	m
51801225	Cl* NGC 6205 ARP 1067	250.513907	36.48670	14.43	12.05	−244.7	4749	1.6	−1.76	1.3	−0.6	4.7	0.91	m
51801203	2MASS J16420943+3633591	250.539279	36.56642	15.08	12.91	−236.4	4998	2.1	−1.63	−3.5	−7.7	8.5	1.00	m
51801215	Cl* NGC 6205 KAD 669	250.582717	36.49612	14.82	12.48	−242.5	4910	1.8	−1.62	−2.0	−6.4	8.1	0.95	m
51807066	2MASS J16502062+3712378	252.585936	37.21049	14.72	12.52	−260.5	5038	2.5	−1.18	−7.9	−0.1	113.3	0.47	h
151410043	2MASS J16552301+3358099	253.845931	33.96943	13.07	10.35	−228.0	4570	1.9	−0.92	−5.6	0.1	224.7	0.92	h
144709105	2MASS J16591121+3326004	254.796675	33.43342	14.96	12.81	−261.0	5070	2.6	−0.75	−0.4	7.8	281.5	0.45	h
151403167	2MASS J16595873+3446331	254.994732	34.77585	14.24	12.06	−214.8	4693	1.5	−1.67	−2.9	4.1	244.8	0.58	h
151007113	2MASS J17043362+3743195	256.140100	37.72209	14.77	12.61	−259.3	5071	2.9	−1.11	−4.3	2.5	283.9	0.50	h

Note. R = radial distance from cluster center.
P_c = membership probability based on V_r.
Status: m—candidate cluster member star; h—candidate extratidal cluster halo star.
Identifications are from Sandage (1970), Barnard (1931), Arp (1955), Kadla (1966), or 2MASS.
[a] Duplicate of 505012198.

fractional mass losses were divided by the corresponding completeness to give total fractional mass losses of 0.0167 for M3 and and 0.0196 for M13.

We then estimated the time taken for a star to move outside our 5° search area. As an estimate, Küpper et al. (2010) Equation (18) gives the relative velocity of escaped stars for clusters in circular orbits in the disk. For M3 this gives a relative velocity of $\pm\sim6.0\,\mathrm{km\,s^{-1}}$ and for M13 $\pm\sim7.3\,\mathrm{km\,s^{-1}}$. As stars can escape in any direction, the mean relative velocities perpendicular to our line of sight (i.e., the proper motions) are $\pm\sim6.0\times2/\pi=\pm\sim3.8\,\mathrm{km\,s^{-1}}$ and $\pm\sim6.0\times2/\pi=\pm\sim4.7\,\mathrm{km\,s^{-1}}$. The stars would move 5° from the GC central position in ∼228 Myr and ∼130 Myr for M3 and M13, respectively, at these velocities.

We divided the fractional mass losses by the time taken for the cluster extratidal halo stars to move outside our search area to give cluster destruction rates. For M3 this was $8.04\times10^{-11}\,\mathrm{yr^{-1}}$ and for M13 our calculated observed destruction rate was $2.47\times10^{-10}\,\mathrm{yr^{-1}}$.

There are several assumptions/estimates in this calculation that should be mentioned: (i) The mass-to-light ratio for the two samples is probably not the same. The integrated cluster luminosity includes a contribution by dwarfs, whereas the observed total luminosity of the cluster extratidal halo stars does not, as they are too faint to detect in LAMOST data. Therefore the observed cluster fractional mass losses are likely underestimated; this would translate to a smaller calculated destruction rate than is actually occuring. (ii) We have made an estimate of DR1 completeness, but this is another possible source of uncertainty. (iii) It is possible that some of the stars we include in our lists of candidates are field stars rather than ex-members of the cluster, so this would lead to an overestimate of cluster destruction rates. (iv) The estimate of the velocities of escaped stars is, as stated, strictly applicable to clusters in circular orbits in the disk; if the actual velocities are lower then the calculated mass-loss rates would also be lower. (v) The velocities of escaped stars are constant. Studies have been done of the variation of V_r along the tidal tail of GCs (e.g., Odenkirchen et al. 2009 and Kuzma et al. 2015 find gradients of $1.0\pm0.1\,\mathrm{km\,s^{-1}\,deg^{-1}}$ for Palomar 5), but without a detailed model for the gravitational potential of the MW's dark matter halo to calculate the orbit of escaped stars, the effect on the destruction rate is difficult to estimate.

Given those limitations in our estimates, our estimated destruction rate for M3 was ∼1–2 orders of magnitude larger than the destruction rates calculated by both Gnedin & Ostriker (1997) and Moreno et al. (2014). For M13, our estimated destruction rate was ∼1 order of magnitude larger than the destruction rates calculated by Gnedin & Ostriker (1997) but ∼3 orders of magnitude larger than those calculated by Moreno et al. (2014).

Differences between our detection of candidate extratidal stars and previous studies of M3 and M13 are not unexpected. M3 observations in particular have produced ambiguous results with Grillmair & Johnson (2006), Jordi & Grebel (2010), and Carballo-Bello et al. (2014) reporting non-detections. However, previous studies are all variations of photometric studies of fairly large numbers of stars. Their analysis used various star counting algorithms and radial density profiles and surface density plots to search for deviations from model profiles and structure or overdensities. These profiles and plots typically did not show deviations or structure much beyond the tidal radius, so the handful of more distant extratidal candidate stars we found would most likely not be detected by these studies.

Finding significant numbers of stars in the process of escaping from these supposedly relatively stable GCs is intriguing. It furthers the case for the existence of extratidal stars associated with M3 as well as affirming the previous positive results for M13. The discrepancies between our observed destruction rates and the predicted rates call for further investigation. To confirm their status our candidate cluster extratidal halo stars require high-resolution spectroscopic observations to match the chemical abundances. The final number confirmed as ex-cluster members can constrain theoretical studies of GC destruction rates as well as the contribution of GCs to the Galaxy's stellar halo. However there are also significant differences in the predicted rates, so the models and simulations are also not yet definitive, and this may also account for some differences.

10. CONCLUSIONS

We find candidate extratidal stars in wide halos around the GCs M3 (NGC 5272) and M13 (NGC 6205) in LAMOST DR1. If their status is confirmed they support previous studies that both clusters are surrounded by a halo of extratidal stars or exhibit tidal tails. Interestingly, destruction rates corresponding to the observed mass loss are generally significantly higher than theoretical studies would indicate. Large-scale spectroscopic surveys such as LAMOST are ideal for this kind of search, especially when combined with photometric and astrometric data. More candidate extratidal stars will almost certainly be found for M3 and M13, and possibly other GCs, as the data set grows, but we support the recommendation of Zhang et al. (2015) to target known photometric members of clusters. High-resolution spectroscopic observations of the candidate extratidal cluster halo stars would be valuable in confirming their origin, and hence provide constraints for theoretical studies.

We thank Borja Anguiano for his assistance and helpful discussions. The authors also thank the reviewer for useful comments and suggestions for improvement. S.L.M. and D.B. Z. acknowledge the financial support from the Australian Research Council through grants DE140100598 and FT110100793, respectively. Guoshoujing Telescope (the Large Sky Area Multi-Object Fiber Spectroscopic Telescope LAMOST) is a National Major Scientific Project built by the Chinese Academy of Sciences. Funding for the project has been provided by the National Development and Reform Commission. LAMOST is operated and managed by the National Astronomical Observatories, Chinese Academy of Sciences. This research made use of NASA's Astrophysics Data System; the VizieR Catalog access tool, CDS, Strasbourg, France; Astropy, a community-developed core Python package for Astronomy (Astropy Collaboration et al. 2013); the IPython package (Pérez & Granger 2007); SciPy (Jones 2001); and TOPCAT, an interactive graphical viewer and editor for tabular data (Taylor 2005). We acknowledge with thanks the variable star observations from the AAVSO International Database contributed by observers worldwide and used in this research. This publication makes use of data products from the Two Micron All Sky Survey, which is a joint project of the University of Massachusetts and the Infrared Processing and Analysis Center/California Institute of

Technology, funded by the National Aeronautics and Space Administration and the National Science Foundation.

Facility: LAMOST.

REFERENCES

Aguilar, L., Hut, P., & Ostriker, J. P. 1988, ApJ, 335, 720
Anguiano, B., De Silva, G. M., Freeman, K., et al. 2016, MNRAS, 457, 2078
Arp, H. C. 1955, AJ, 60, 317
Astropy Collaboration, Robitaille, T. P., Tollerud, E. J., et al. 2013, A&A, 558, A33
Barnard, E. E. 1931, PYerO, 6, 1
Baumgardt, H., & Makino, J. 2003, MNRAS, 340, 227
Bellazzini, M., Ibata, R., & Ferraro, F. R. 2004, in ASP Conf. Ser. 327, Satellites and Tidal Streams, ed. F. Prada, D. Martinez Delgado, & T. J. Mahoney, (San Francisco, CA: ASP), 220
Bressan, A., Marigo, P., Girardi, L., et al. 2012, MNRAS, 427, 127
Bullock, J. S., & Johnston, K. V. 2005, ApJ, 635, 931
Carballo-Bello, A. J., Martínez-Delgado, D., & Sollima, A. 2011, in EAS Publications Ser. 48, 351
Carballo-Bello, J., Sollima, A., Martinez-Delgado, D., et al. 2014, MNRAS, 445, 2971
Chen, C. W., & Chen, W. P. 2010, ApJ, 721, 1790
Chernoff, D. F., Kochanek, C. S., & Shapiro, S. L. 1986, ApJ, 309, 183
Cohen, J. G., & Meléndez, J. 2005, AJ, 129, 303
Da Costa, G. S. 2015, arXiv:1510.00873
Dinescu, D., Girard, T., & van Altena, W. 1999, AJ, 117, 1792
Frinchaboy, P. M., & Majewski, S. R. 2008, AJ, 136, 118
Gnedin, O., & Ostriker, J. 1997, ApJ, 474, 223
Gratton, R. G., Carretta, E., & Bragaglia, A. 2012, A&ARv, 20, 50
Grillmair, C. J., Ajhar, E. A., Faber, S. M., et al. 1996, AJ, 111, 2293
Grillmair, C. J., & Dionatos, O. 2006, ApJL, 641, L37
Grillmair, C. J., Freeman, K. C., Irwin, M., & Quinn, P. J. 1995, AJ, 109, 2553
Grillmair, C. J., & Johnson, R. 2006, ApJL, 639, L17
Harris, W. 1996, AJ, 112, 1487
Henden, A. A., Welch, D. L., Terrell, D., & Levine, S. E. 2009, BAAS, 41, 669
Hut, P., & Djorgovski, S. 1992, Natur, 359, 806
Johnson, C. I., & Pilachowski, C. A. 2012, ApJL, 754, L38
Jones, E. 2001, SciPy: Open source scientific tools for Python
Jordi, K., & Grebel, E. 2010, A&A, 522, A71
Kadla, E. I. 1966, IzPul, 181, 93
Kharchenko, N. V., Piskunov, A. E., Schilbach, E., Röser, S., & Scholz, R.-D. 2013, A&A, 558, A53
Koposov, S. E., Rix, H.-W., & Hogg, D. W. 2010, ApJ, 712, 260
Kunder, A., Bono, G., Piffl, T., et al. 2014, A&A, 572, A30
Küpper, A., Balbinot, E., Bonaca, A., et al. 2015, ApJ, 803, 80
Küpper, A. H. W., Kroupa, P., Baumgardt, H., & Heggie, D. C. 2010, MNRAS, 401, 105
Kuzma, P. B., Da Costa, G. S., Keller, S. C., & Maunder, E. 2015, MNRAS, 446, 3297
Lehmann, I., & Scholz, R.-D. 1997, A&A, 320, 776
Leon, S., Meylan, G., & Combes, F. 2000, A&A, 359, 907
Luo, A., Zhao, Y., Zhao, G., et al. 2015, arXiv:1505.01570
Mackey, A. D., & Gilmore, G. F. 2004, MNRAS, 355, 504
Mackey, A. D., & van den Bergh, S. 2005, MNRAS, 360, 631
Marin-Franch, A., Aparicio, A., Piotto, G., et al. 2009, ApJ, 694, 1498
Marino, A. F., Milone, A. P., Yong, D., et al. 2014, MNRAS, 442, 3044
Martell, S. L., & Grebel, E. K. 2010, A&A, 519, A14
Martell, S. L., Smolinski, J. P., Beers, T. C., & Grebel, E. K. 2011, A&A, 534, A136
McLaughlin, D. E., & van der Marel, R. P. 2005, ApJS, 161, 304
Moreno, E., Pichardo, B., & Velázquez, H. 2014, ApJ, 793, 110
Navin, C., Martell, S., & Zucker, D. 2015, MNRAS, 453, 531
Odenkirchen, M., Grebel, E. K., Kayser, A., Rix, H.-W., & Dehnen, W. 2009, AJ, 137, 3378
Pérez, F., & Granger, B. E. 2007, CSE, 9, 21
Robin, A. C., Reylé, C., Derrière, S., & Picaud, S. 2003, A&A, 409, 523
Sandage, A. 1970, ApJ, 162, 841
Sandage, A., & Katem, B. 1982, AJ, 87, 537
Sandage, A. R. 1953, AJ, 58, 61
Sharma, S., Bland-Hawthorn, J., Johnston, K. V., & Binney, J. 2011, ApJ, 730, 3
Skrutskie, M., Cutri, R., Stiening, R., et al. 2006, ApJ, 131, 1163
Taylor, M. B. 2005, in ASP Conf. Ser. 347, Astronomical Data Analysis Software and Systems XIV, ed. P. Shopbell, M. Britton, & R. Ebert, (San Francisco, CA: ASP), 29
Vesperini, E. 1997, MNRAS, 287, 915
Zacharias, N., Finch, C. T., Girard, T. M., et al. 2013, AJ, 145, 44
Zhang, B., Chen, X.-Y., Liu, C., et al. 2015, RAA, 15, 1197
Zhao, G., Chen, Y.-Q., Shi, J.-R., et al. 2006, ChJAA, 6, 265

Search Results

The Astrophysical Journal

Title Details

Related Titles

▶ **Alternative Media Edition** (2)

Lists

Marked Titles (0)

Search History

1538-4357 - (1)

▼ **Basic Description**

Title	The Astrophysical Journal
ISSN	1538-4357
Publisher	Institute of Physics Publishing, Inc.
Country	United States
Status	Active
Frequency	18 times a year
Language of Text	Text in: English
Refereed	Yes
Abstracted / Indexed	Yes
Serial Type	Journal
Content Type	Academic / Scholarly
Format	Online
Website	http://iopscience.iop.org/0004-637X/
Description	Devoted to recent developments, discoveries, and theories in astronomy and astrophysics.

▶ **Subject Classifications**

▶ **Additional Title Details**

▶ **Title History Details**

▶ **Publisher & Ordering Details**

▶ **Price Data**

▶ **Online Availability**

▶ **Abstracting & Indexing**

▶ **Other Availability**

▶ **Demographics**

Save to List Email Download Print Corrections Expand All Collapse All